Sustainable Interface Regulation Enabled by Bismuth Solid-State Surfactant Effect for Zn-free Anodes

Chen Wang,‡[a] Bo Chen,‡[a] Tan Wang,[a] Gabriel Vinicius De Oliveira Silva,[c] Zhi Xu,[d] Guo-Xing Miao,*[c] Yunhui Huang,*[e] and Jing Fu*[ab]

[a] *School of Materials Science and Engineering, Tongji University, Shanghai 201804, P. R. China.*
[b] *Shanghai Key Laboratory of Development & Application for Metallic Functional Materials, Shanghai, China.*
[c] *Institute for Quantum Computing, Department of Electrical and Computer Engineering, University of Waterloo, Ontario, Canada.*
[d] *Beijing National Laboratory for Condensed Matter Physics, Institute of Physics, Chinese Academy of Sciences, Beijing, China.*
[e] *School of Materials Science and Engineering, Huazhong University of Science and Technology, Wuhan, China.*
† Electronic Supplementary Information (ESI) available: Supplementary figures and tables in this study. See DOI: 10.1039/x0xx00000x
‡ These authors contributed equally to this work.

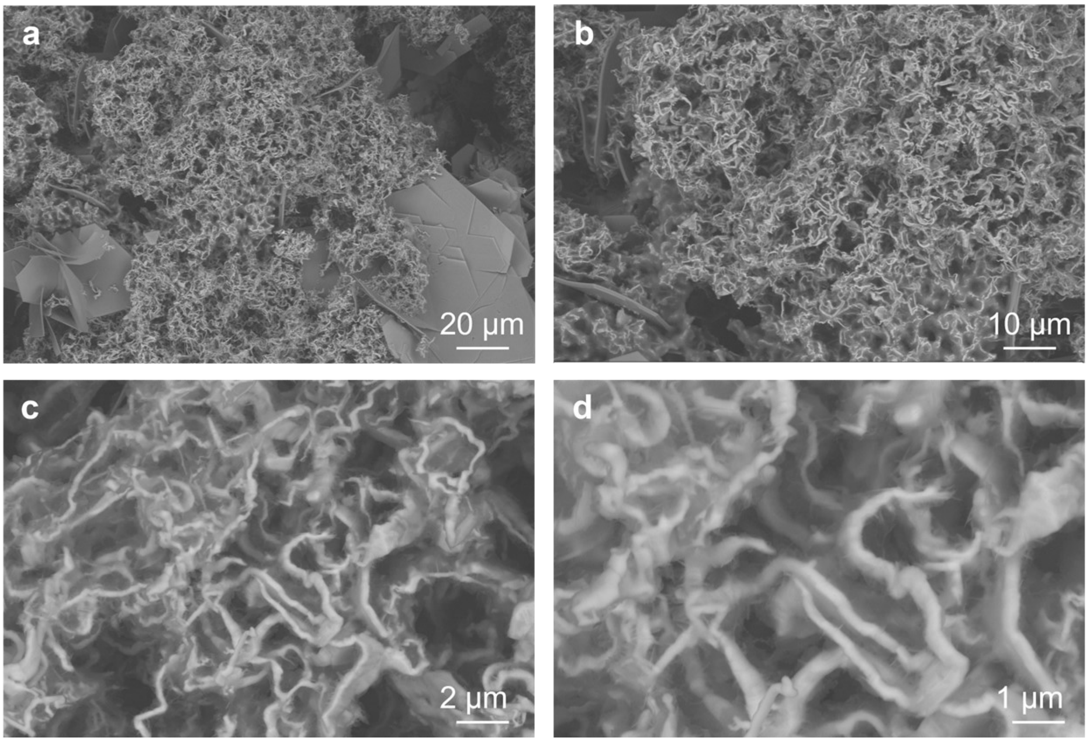

Supplementary Fig. 1 (a-d) SEM images of the plated Zn on bare Zn electrode with varied magnifications from a three-electrode cell system at 5 mA cm^{-2}.

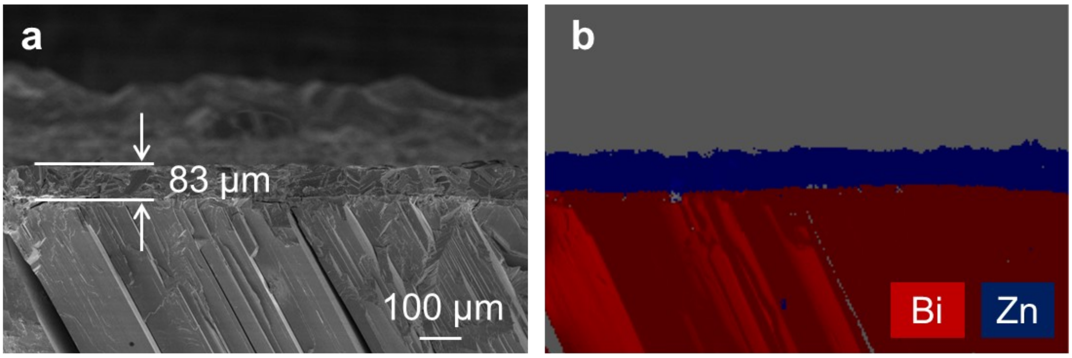

Supplementary Fig. 2 (a) Cross-sectional SEM image and (b) corresponding EDX elemental mapping of Zn film deposited on Bi electrode at 5 mA cm^{-2} with a capacity of 50 mAh cm^{-2}.

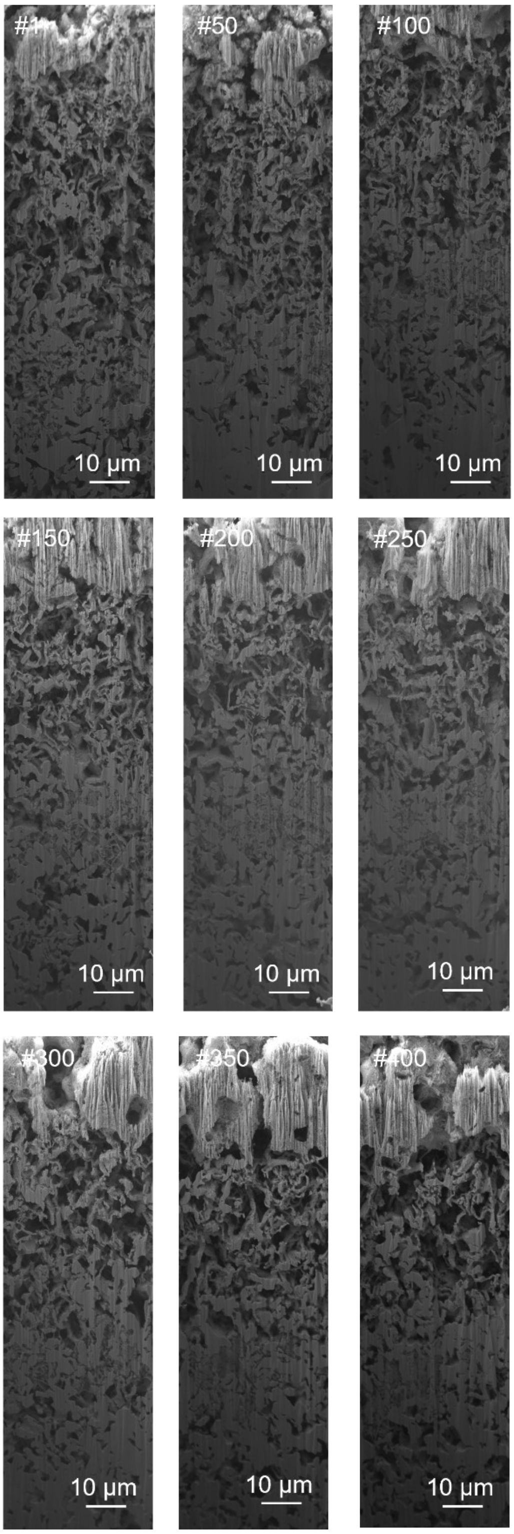

Supplementary Fig. 3 Cross-sectional SEM images of Zn deposited on Zn electrode through serial cross-sectional FIB cuts. The distance between each cross-sectional SEM image is 150 nm.

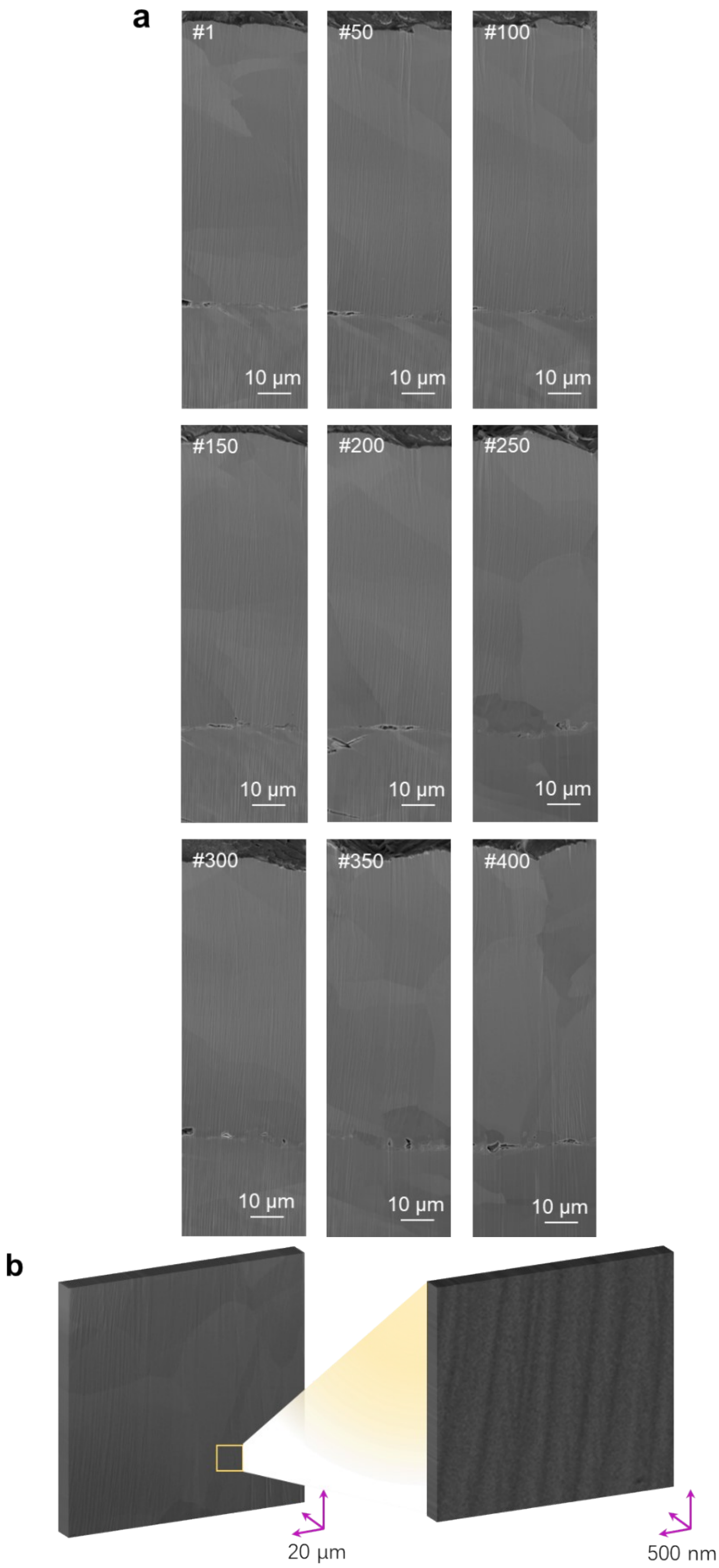

Supplementary Fig. 4 (a) Cross-sectional SEM images and (b) local magnification of Zn deposited on Bi electrode after plating 50 mAh cm^{-2} through serial cross-sectional FIB cuts. The distance between each cross-sectional SEM image is 150 nm.

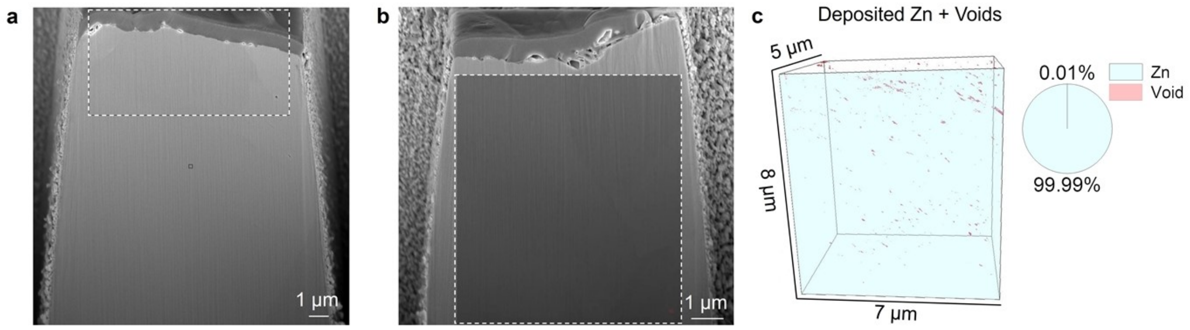

Supplementary Fig. 5 (a-b) Cross-sectional images of Zn deposits on Bi substrate produced by FIB with the selected position for 3D morphology reconstruction. (c) 3D reconstruction of deposited Zn (green) and voids (red) from 400 images of (b).

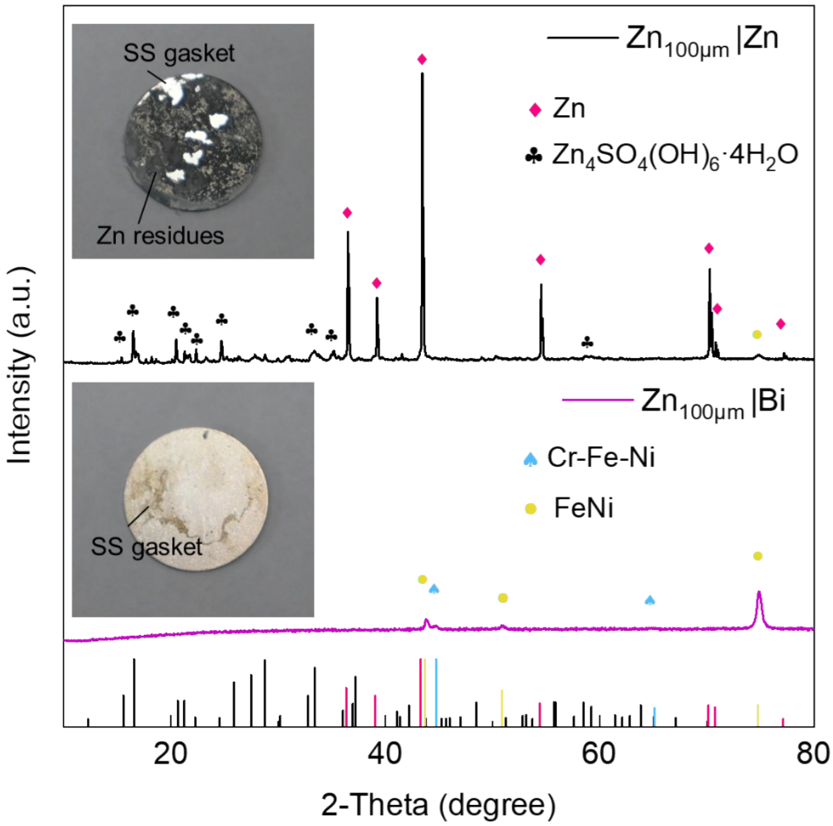

Supplementary Fig. 6 XRD patterns and corresponding photos (insert) of the working electrode sides including stainless-steel gaskets from disassembled coin cells.

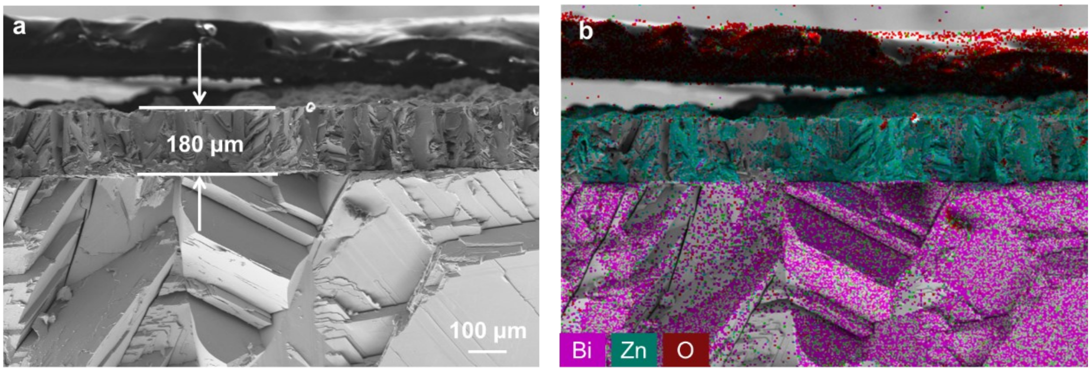

Supplementary Fig. 7 (a) Cross-sectional SEM image and (b) corresponding EDX mapping of Zn film deposited on Bi electrode at a capacity of 115 mAh cm^{-2}.

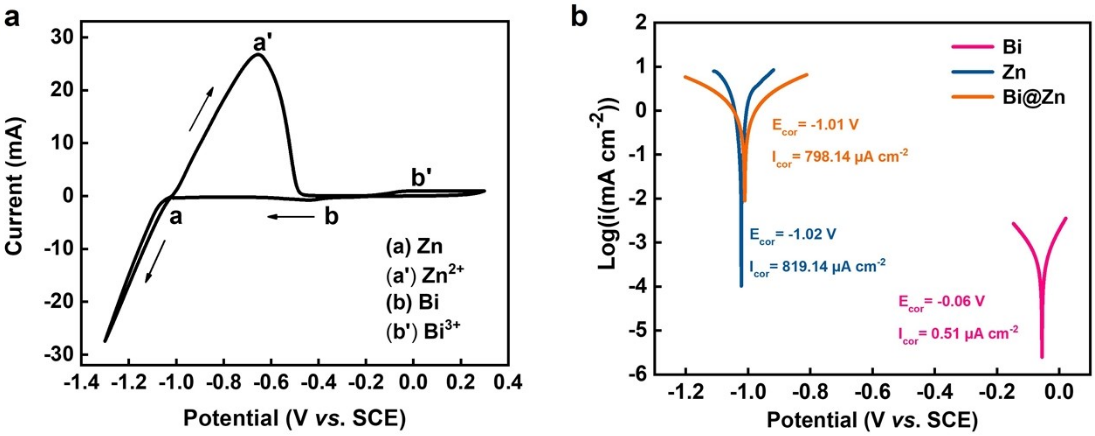

Supplementary Fig. 8 (a) CV curve of the Bi working electrode tested in the three-electrode system within a voltage window including the redox reactions of Zn and Bi. (b) Tafel plots of Bi and Zn working electrodes in 2 M $ZnSO_4$ electrolytes under the three-electrode system.

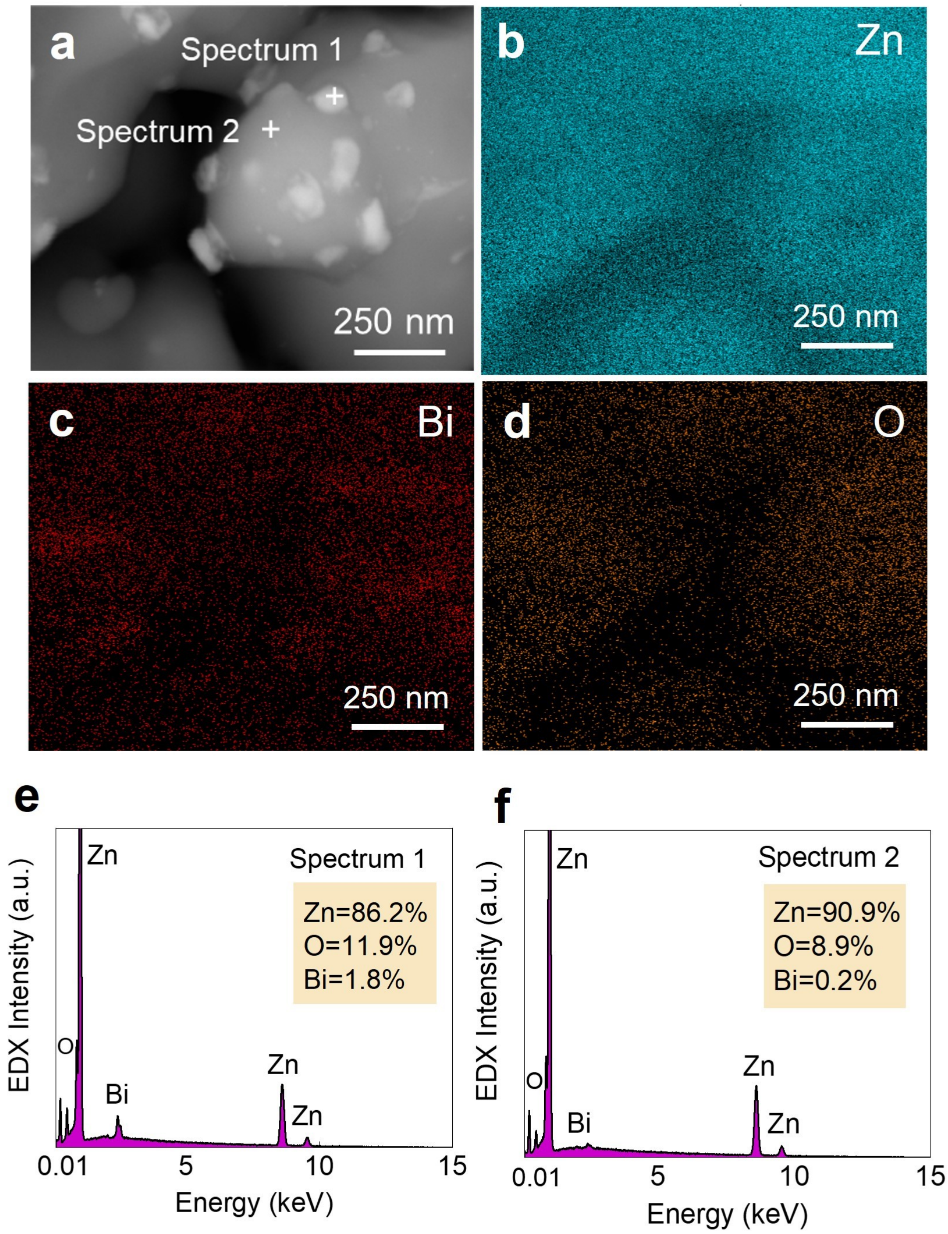

Supplementary Fig. 9 (a) SEM image and (b-d) corresponding EDX area maps of Zn deposits for a capacity of 5 mAh cm^{-2}. (e-f) EDX spectra recorded by spot analysis at two points marked on the particle in a.

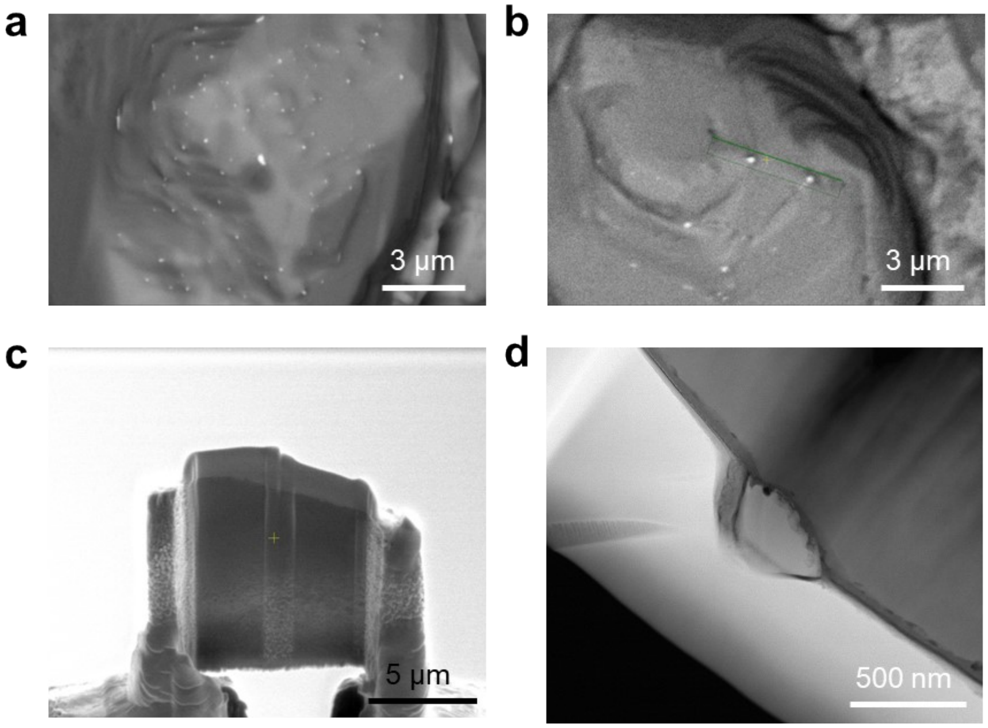

Supplementary Fig. 10 (a) SEM image of Zn plated on Bi foil with a capacity of 5 mAh cm^{-2} before FIB slicing. (b) SEM image of the FIB sliced region. (c) TEM lamella by FIB and (d) the TEM image of the selected region with a Bi particle.

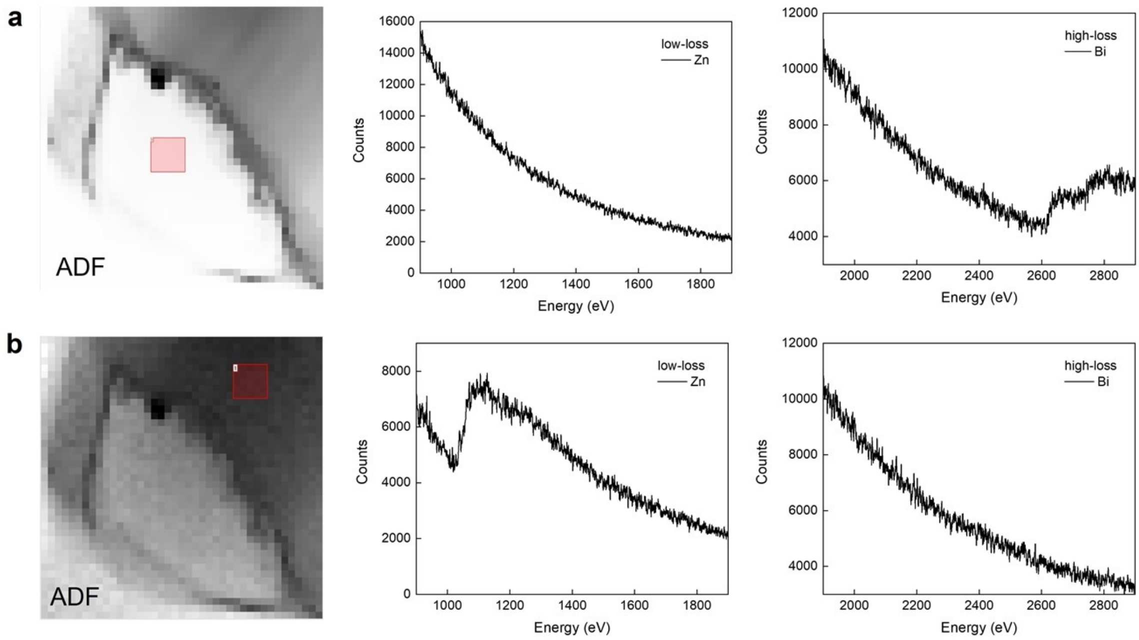

Supplementary Fig. 11 The ADF-STEM images and the corresponding EELS spectra of selected region on (a) Bi and (b) Zn particles.

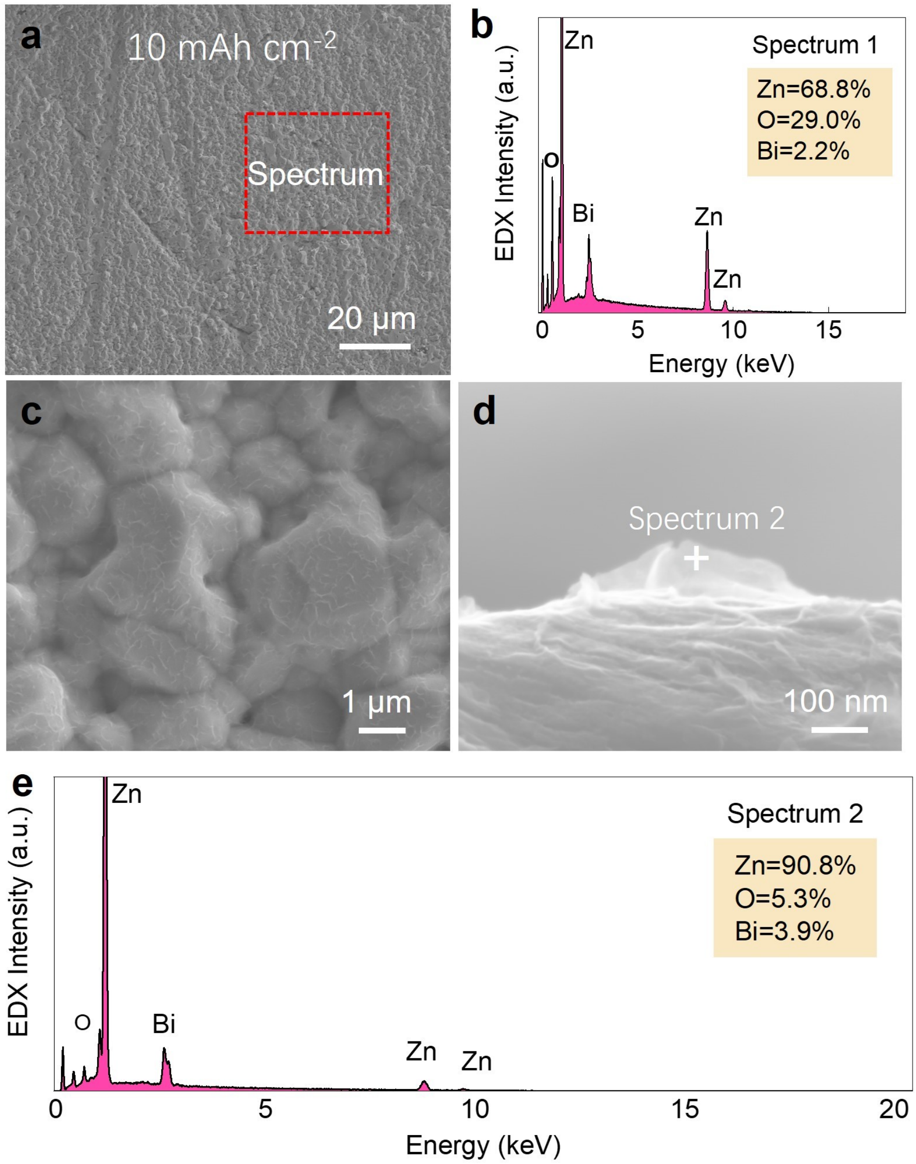

Supplementary Fig. 12 (a,c,d) SEM images of Zn plated on Bi electrode with a capacity of 10 mAh cm^{-2}. (b,d) The qualitative area and spot scan EDX analysis.

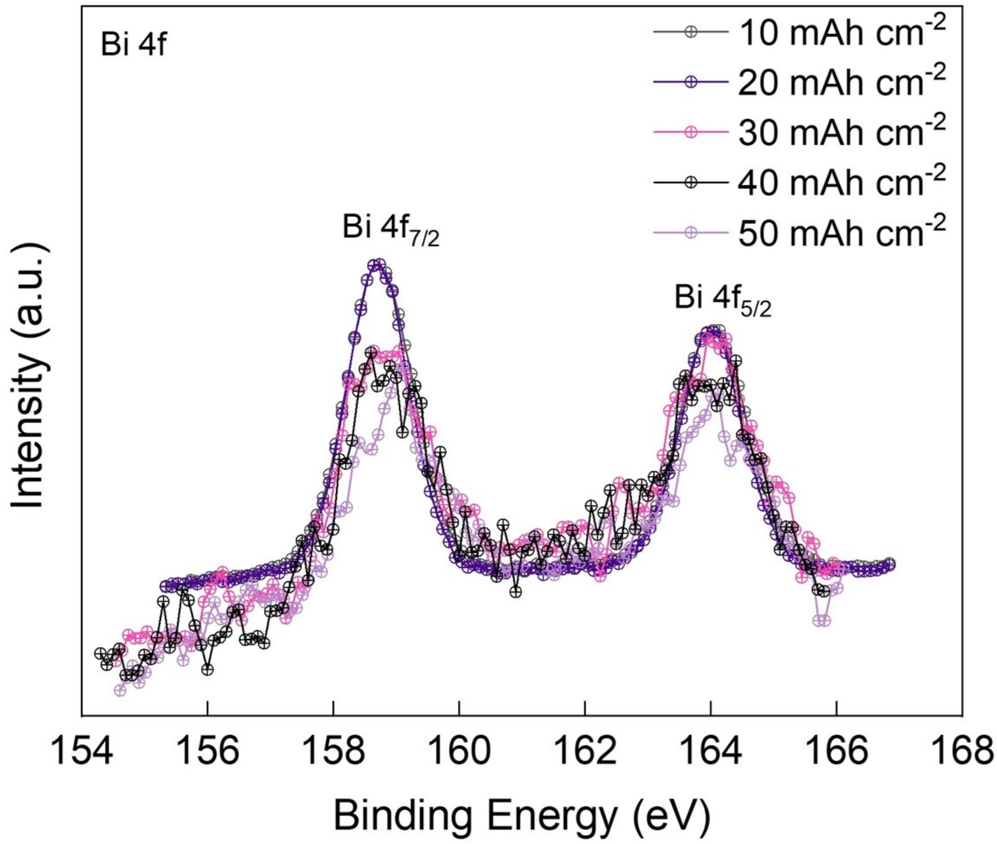

Supplementary Fig. 13 High-resolution XPS spectra of Bi 4f for electrodes with different Zn plating capacities.

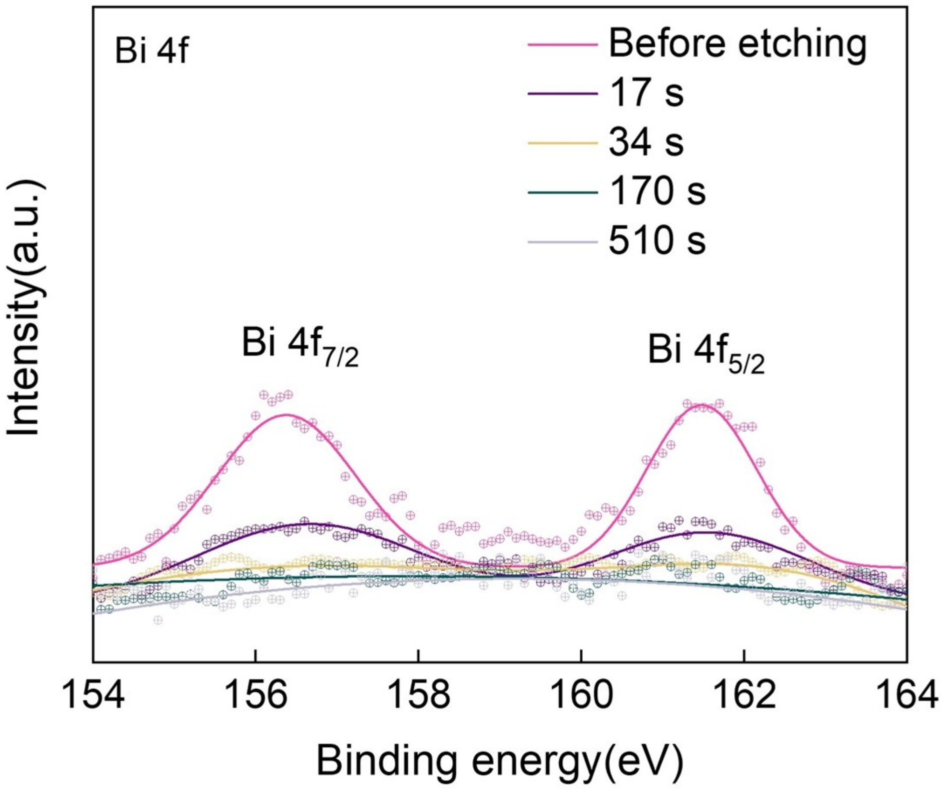

Supplementary Fig. 14 XPS depth profile analysis of plated Zn with a capacity of 10 mAh cm^{-2}.

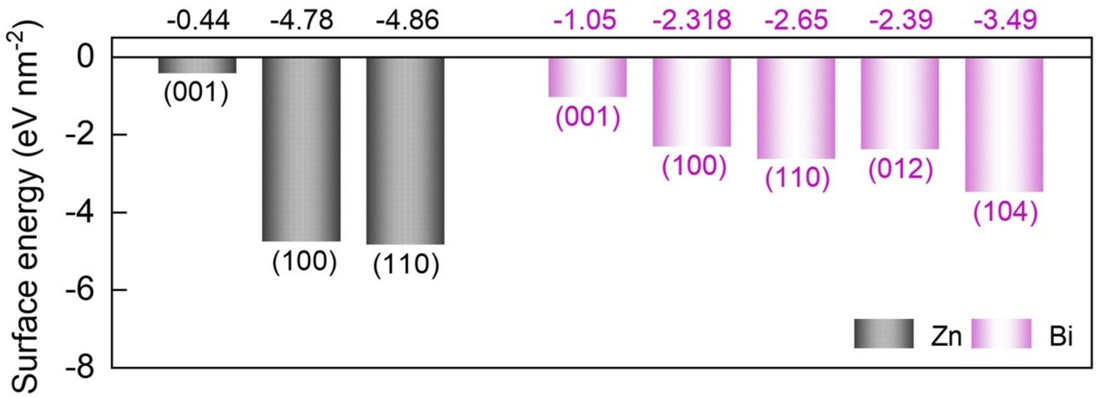

Supplementary Fig. 15 The calculated surface energies for Zn and Bi.

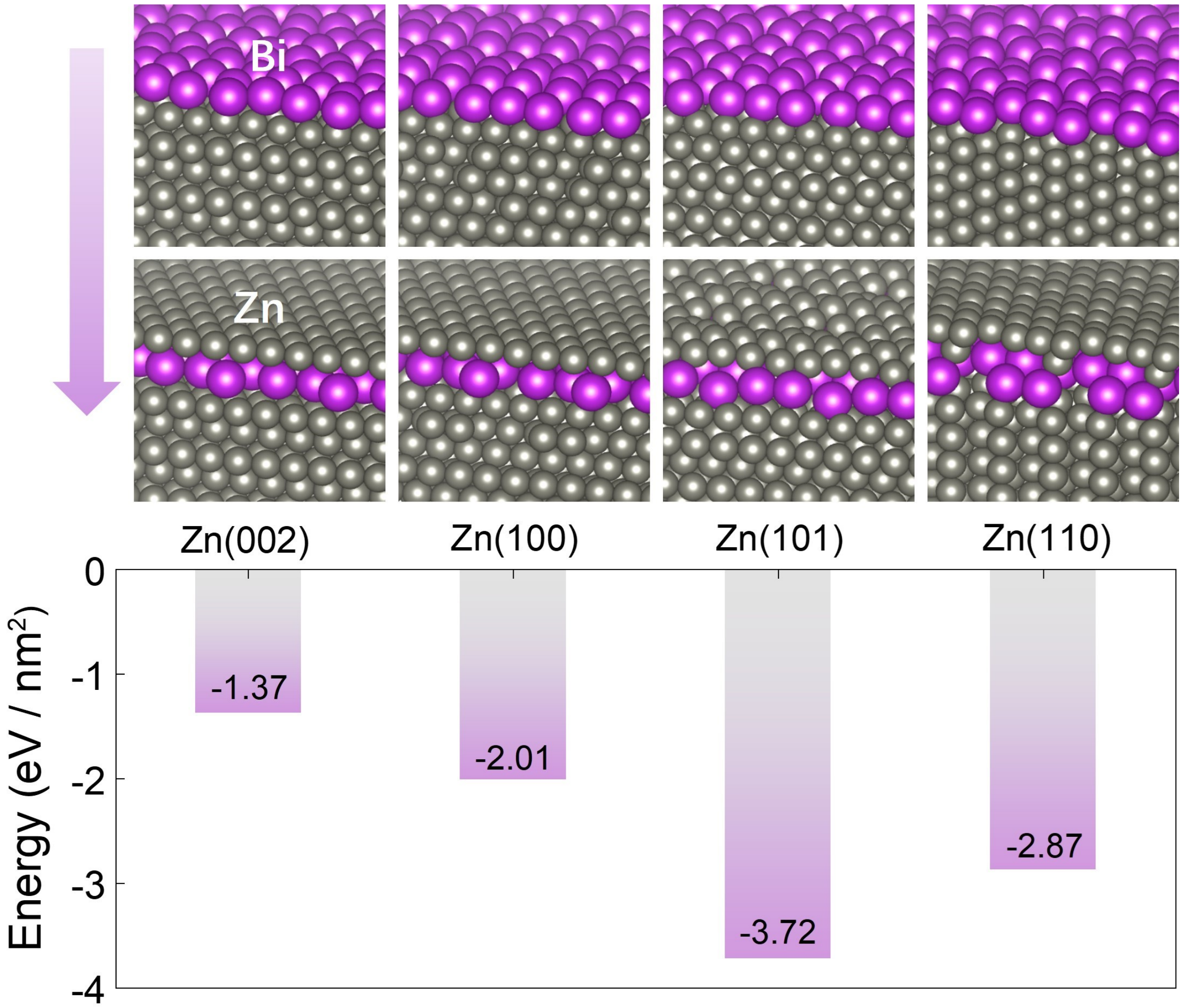

Supplementary Fig. 16 DFT calculation of one monolayer of Bi floating on 6 atomic layers of Zn, compared to it inserted beneath one atomic layer of Zn. The numbers indicate the corresponding reduction energy for different Zn orientations (top vs. bottom configuration).

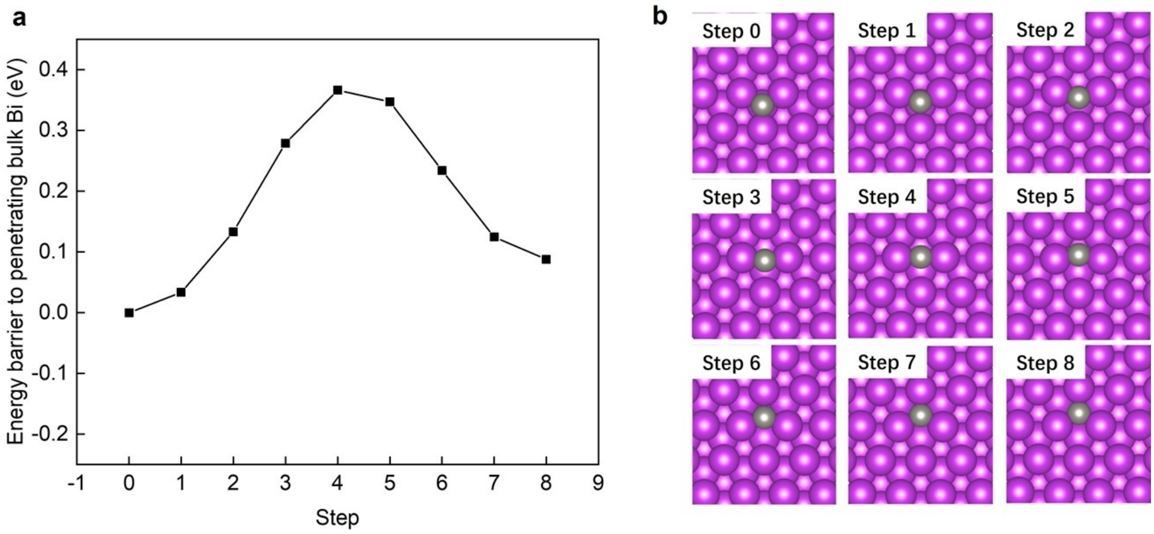

Supplementary Fig. 17 (a) Energy barrier for Zn to penetrate a bulk Bi crystal calculated by DFT. (b) Sectional views of Zn atom migration in a Bi crystal by DFT modeling.

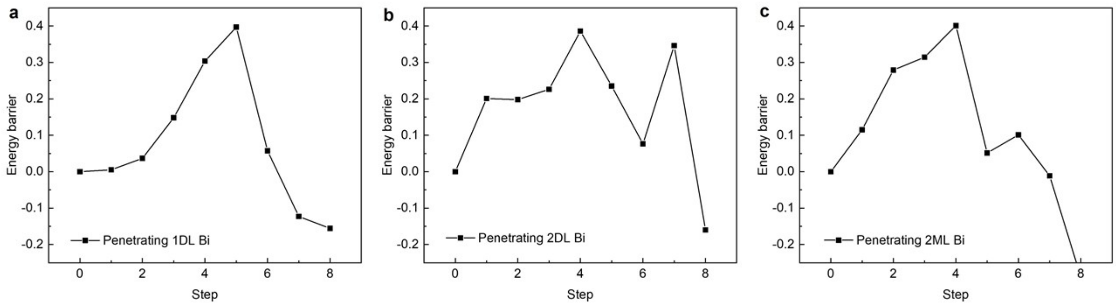

Supplementary Fig. 18 The migration barriers for Zn to penetrate the Bi coverage layers by covering (a) one double layer of Bi, (b) two double layers of Bi and (c) two monolayers of amorphous Bi on top of Zn (001) surface.

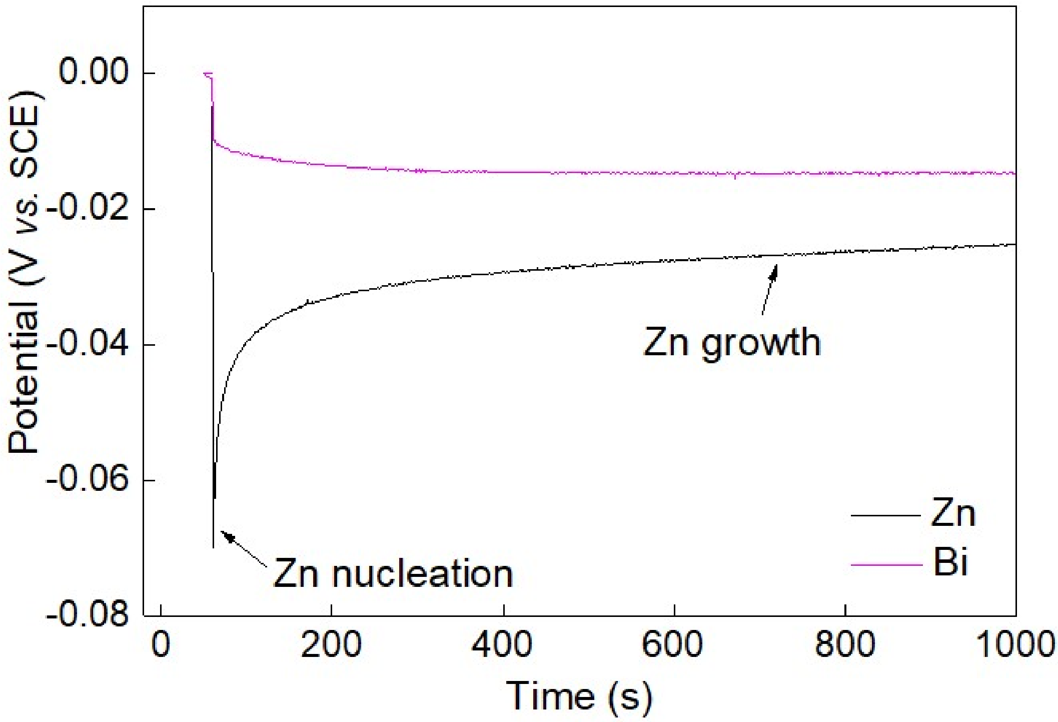

Supplementary Fig. 19 Galvanostatic discharge profiles of Zn plating on Bi and Zn working electrodes in the three-electrode systems.

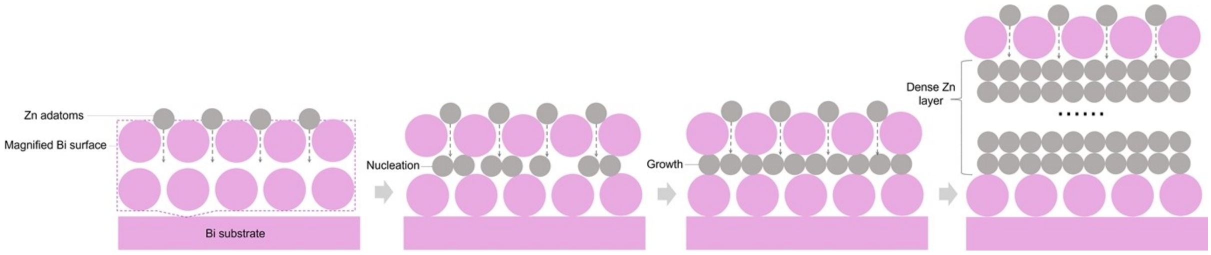

Supplementary Fig. 20 Mechanism of dense Zn deposition layer formation through dynamic regulation by Bi solid-state surfactant.

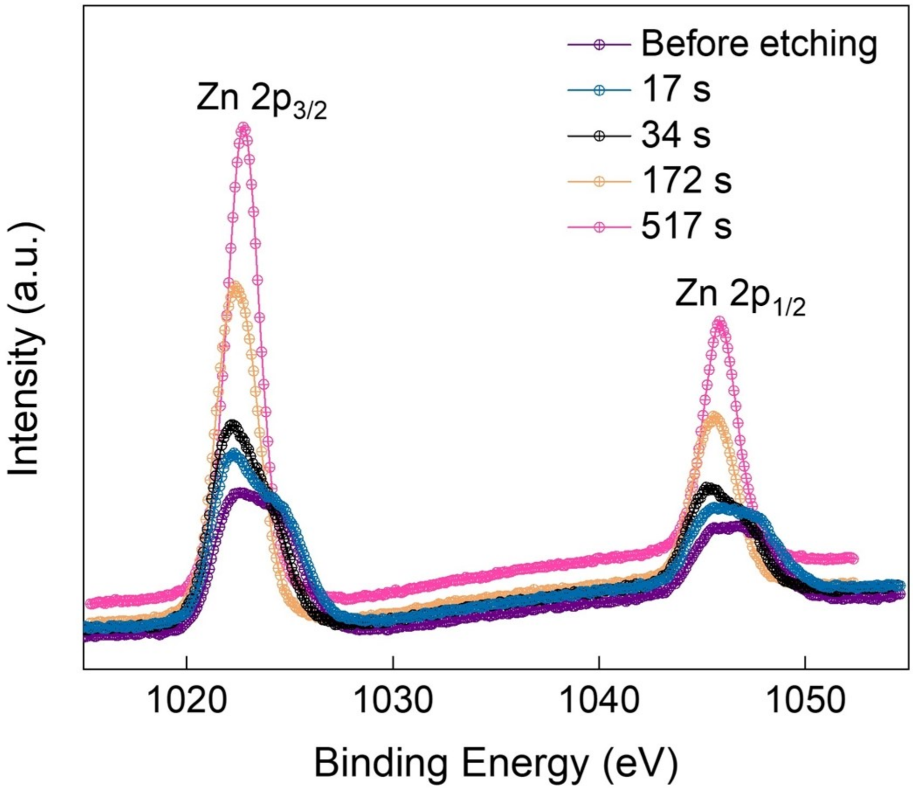

Supplementary Fig. 21 XPS depth profile analysis of plated Zn with a capacity of 10 mAh cm^{-2}.

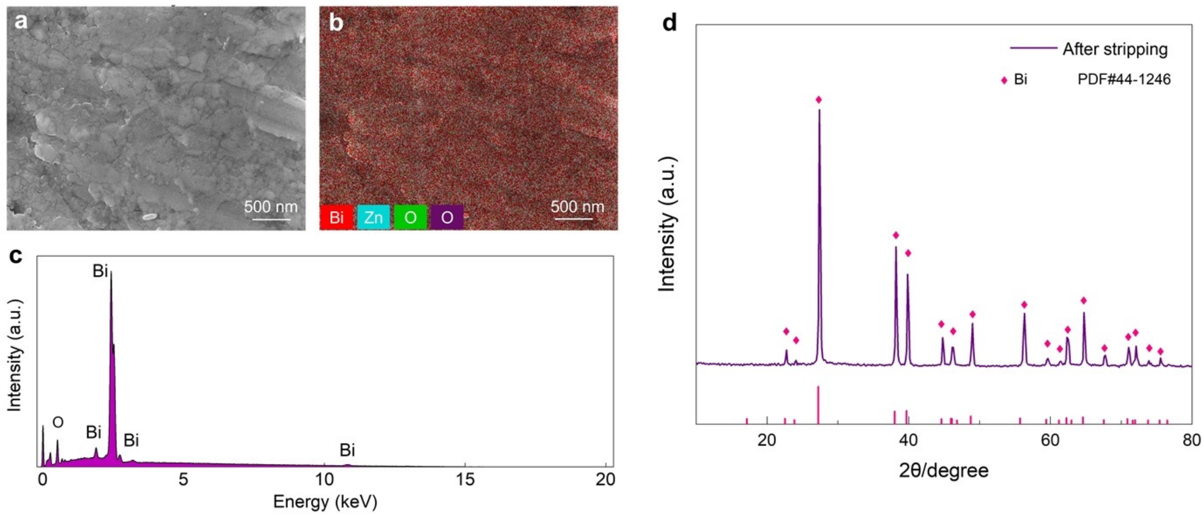

Supplementary Fig. 22 (a) SEM image, (b) EDX elemental mapping, (c) the qualitative area scan EDX analysis and (d) XRD pattern of the full stripped Bi electrode.

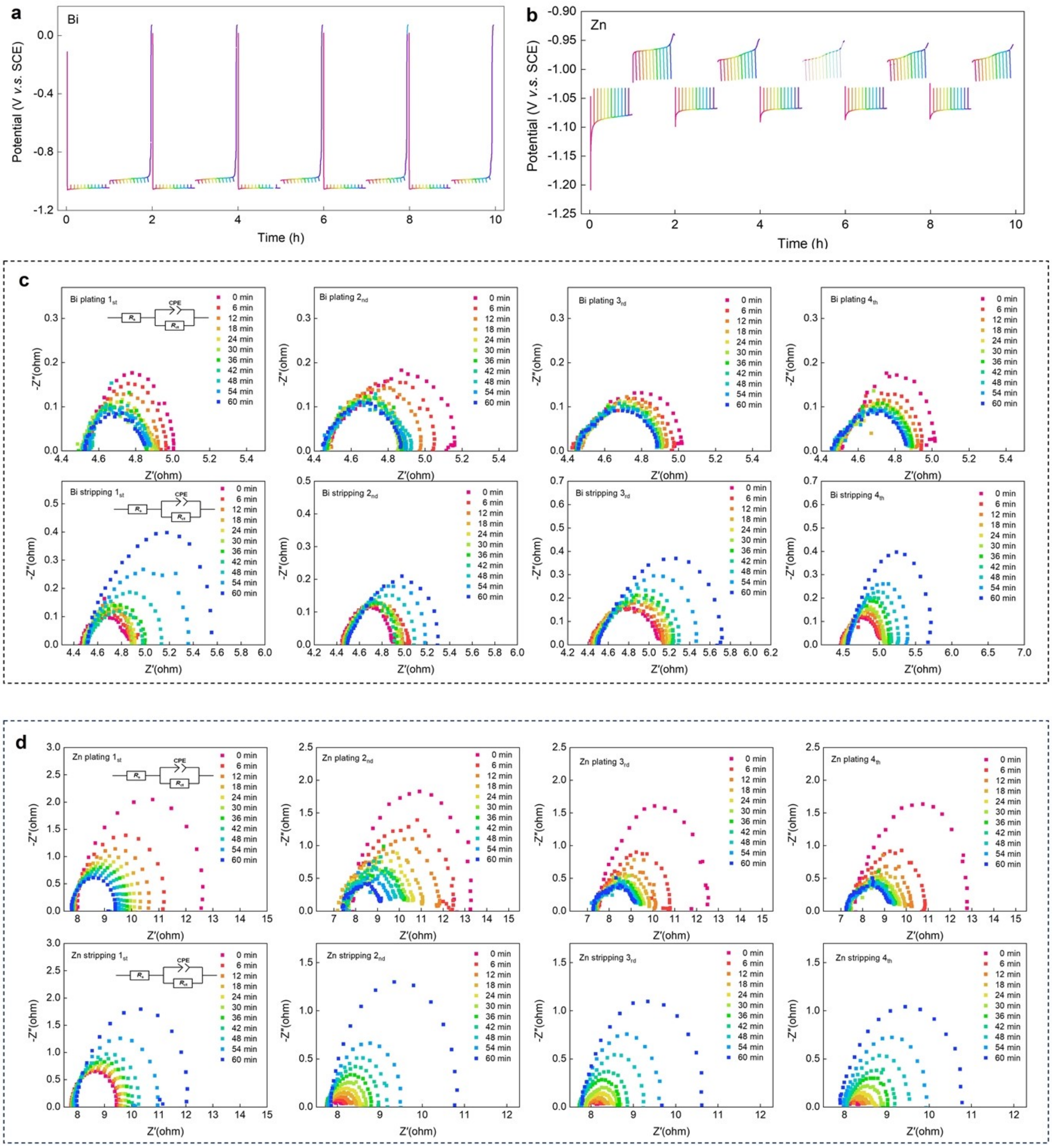

Supplementary Fig. 23 The in-situ EIS-coupled galvanostatic charge-discharge curves of (a) Bi and (b) Zn as the working electrodes at 5 mA cm^{-2} in the three-electrode system. In-situ Nyquist plots of (c) Bi and (d) Zn as the working electrodes under plating and stripping states at different cycles.

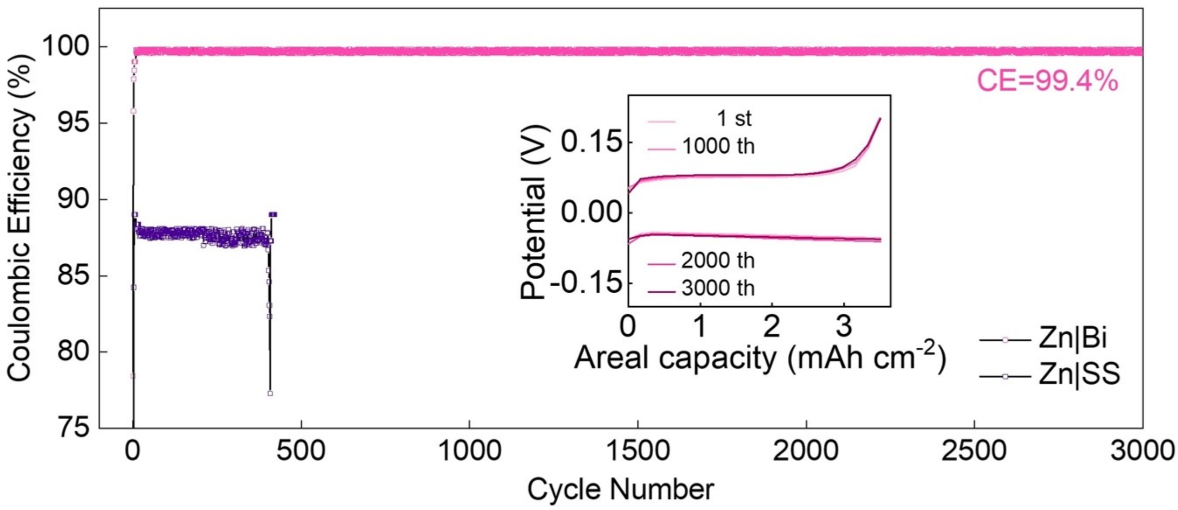

Supplementary Fig. 24 Cycling stability of different asymmetric cell configurations with an areal capacity of 3.5 mAh cm^{-2}. The inset is voltage profiles of selected cycles for Zn|Bi cell.

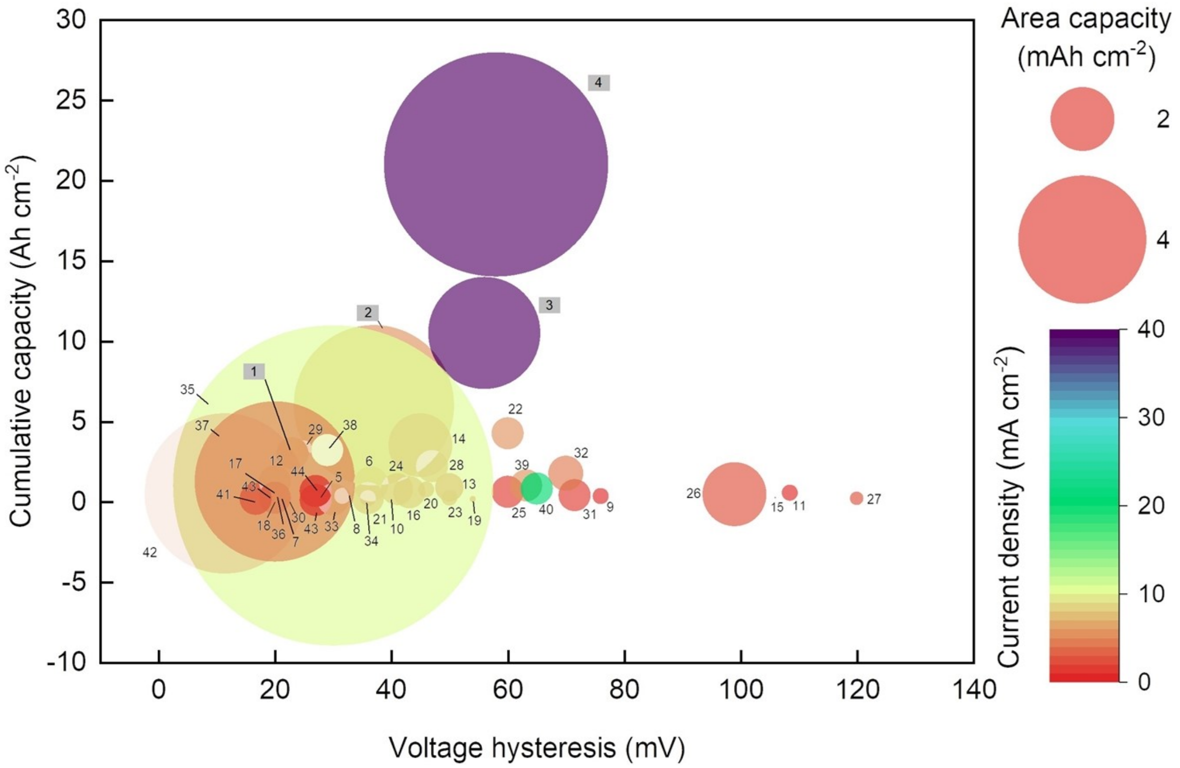

Supplementary Fig. 25 Performance comparison of recent three works based on different anode modification strategies.

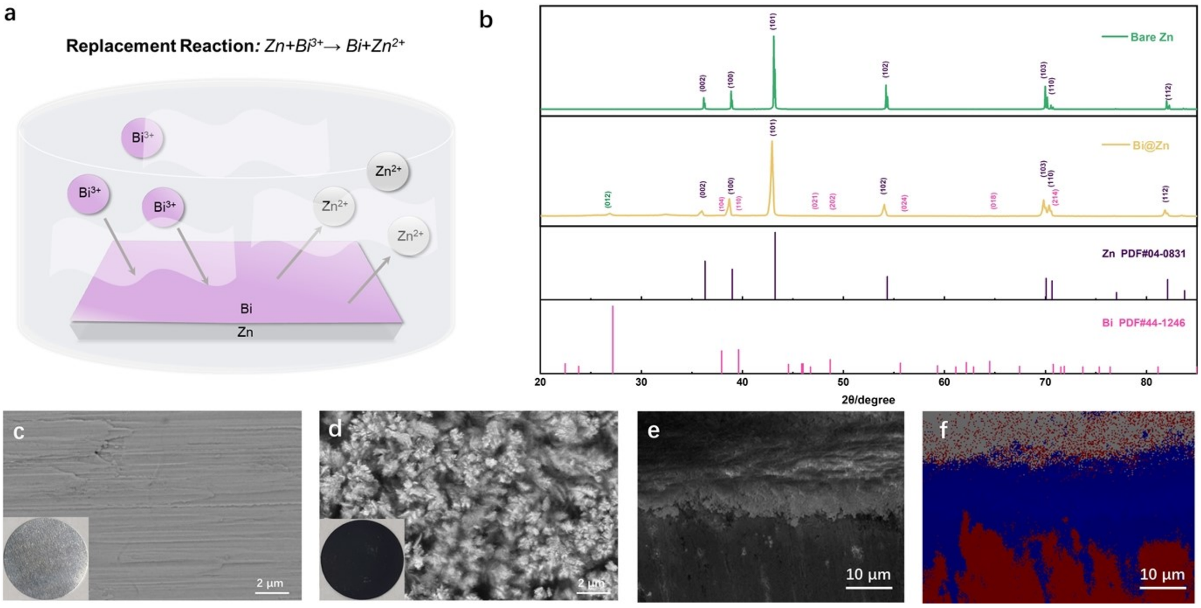

Supplementary Fig. 26 (a) Schematic illustration of the Bi@Zn electrode prepared by a replacement reaction. (b) XRD patterns of bare Zn and Bi@Zn electrodes. SEM images of (c) bare Zn and (d) Bi@Zn electrodes (insets are photos of the electrodes). (e) Cross sectional SEM image and (f) EDX mapping of Bi@Zn.

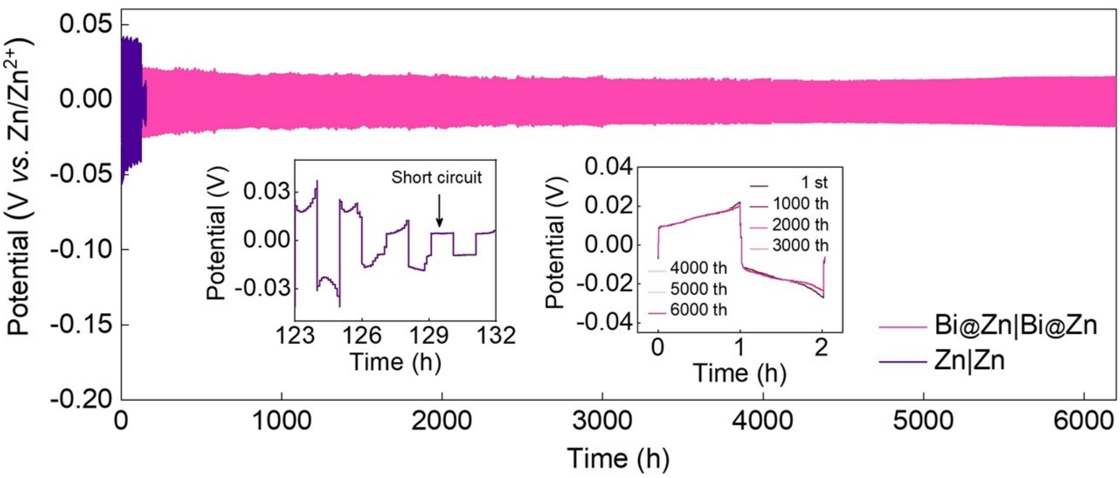

Supplementary Fig. 27 Cycling stability of different symmetric cell configurations with an areal capacity of 1 mAh cm^{-2}. The insets are magnified views of selected cycles for Zn|Zn (left) and Bi@Zn|Bi@Zn cells (right).

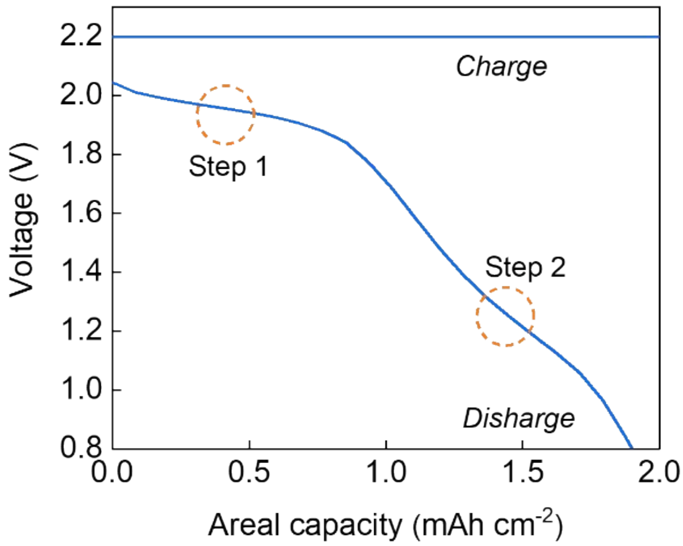

Supplementary Fig. 28 Galvanostatic discharge curve of Bi|CC cell for the charge capacity of 2 mAh cm^{-2}.

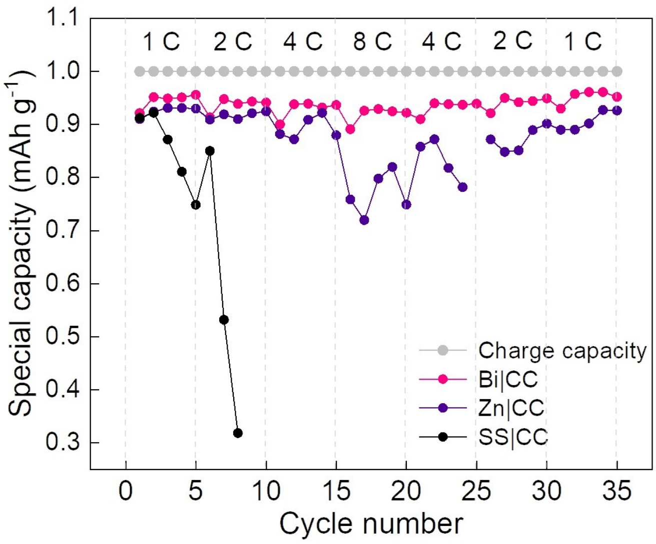

Supplementary Fig. 29 Rate performance of full cells using different anodes at an areal capacity of 1 mAh cm^{-2}.

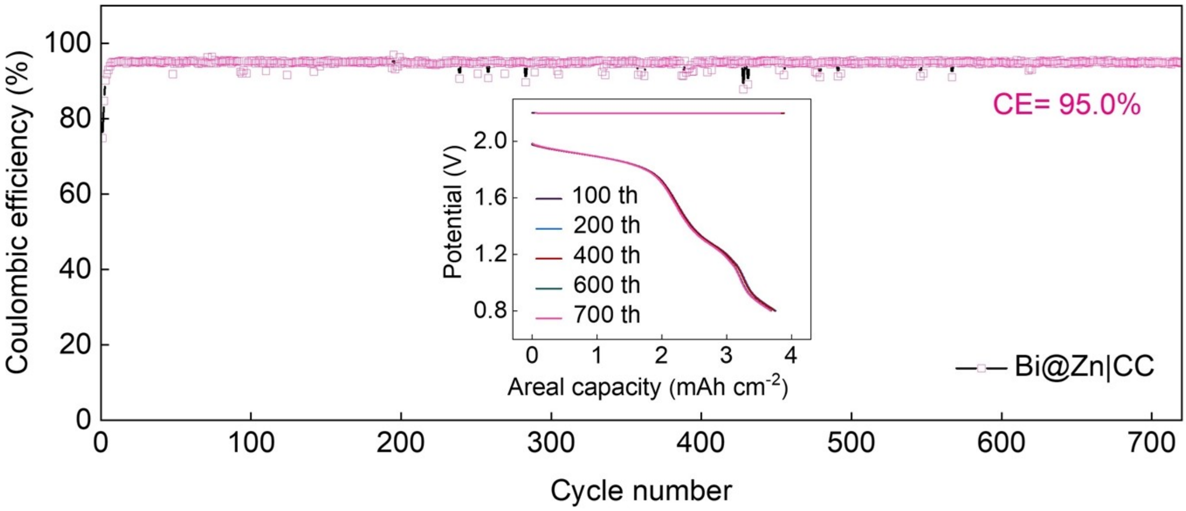

Supplementary Fig. 30 CE of the full cell using Bi@Zn as negative electrode at an areal capacity of 4 mAh cm^{-2} (inset is voltage profiles of selected cycles for Bi@Zn|CC cell).

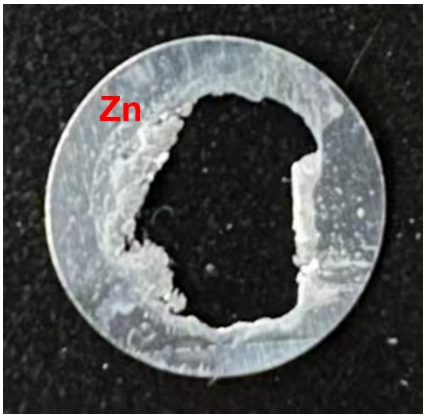

Supplementary Fig. 31 The photo of the highly corroded Zn anode after 100 cycles.

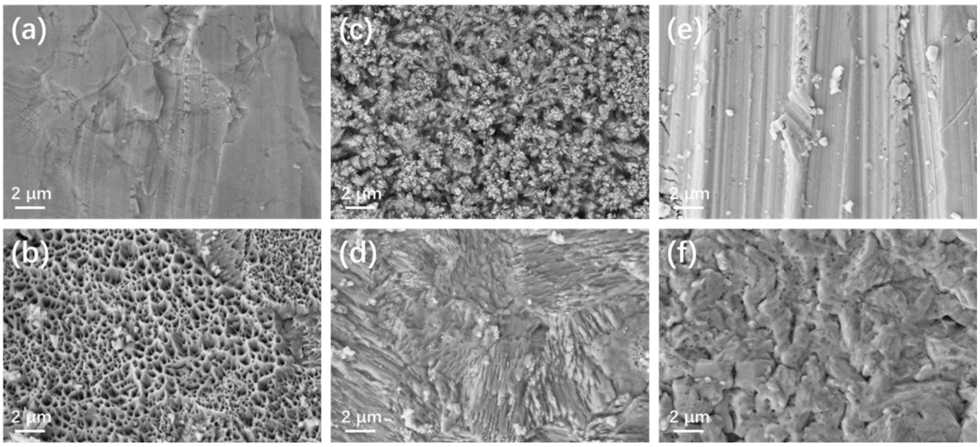

Supplementary Fig. 32 The SEM images of fresh anode surfaces of (a) Zn, (c) Bi@Zn, and (e) Bi, respectively. SEM images of cycled anodes of (b) Zn, (d) Bi@Zn, and (f) Bi (conditions: after cycled for 20 cycles and then stopped at the Zn deposition step with a capacity of 4 mAh cm^{-2}).

Supplementary Table 1. Performance comparison of recent three works based on different anode modification strategies.

NO.	Strategy*	Voltage hysteresis (mV)	CE (%)	Life (h or cycles)	Cumulative capacity (Ah cm^{-2})	Current density (mA cm^{-2})	Areal capacity (mAh cm^{-2})	Ref.
1	Bi@Zn	23	-	6000 h	3	1	1	This work
2	Bi@Zn	37	-	2400 h	6	5	5	This work
3	Bi	56	99.4	3000 cycles	10.5	3.5	40	This work
4	Bi	58	98.7	3000 cycles	21	7	40	This work
5	COP-CMC/QG	28	-	4000 h	0.5	0.05	0.25	[1]
		-	99.0	490 cycles	0.245	0.5	1	
6	Mesoporous TiO_2	36.5	98.95	500 h	1.1	1.1	4.4	[2]
7	γ-Al_2O_3	21	-	300 h	0.15	0.5	1	[3]
8	Mg–Al LDH	31.6	-	1400 h	0.35	0.5	0.5	[4]
		-	99.2	2000 cycles	2	1	10	
9	MXene and chitosan mixtur	76	99	1350 h	0.3375	0.5	0.5	[5]
10	β-PVDF	40	-	2000 h	0.25	0.05	0.25	[6]
		-	96.5	200 cycles	0.036	0.18	0.36	
11	PVB	108.5	-	2200 h	0.55	0.5	0.5	[7]
		-	99.4	100 cycles	0.2	2	4	
12	NiCo-LDH	20	-	2500 h	1.25	1	1	[8]
		-	99.0	700 cycles	0.7	1	2	
13	AEC	50	-	2000 h	0.885	0.885	0.885	[9]
		-	99.4	1000	0.885	0.885	1.77	
14	SIR	45	-	3500 h	3.5	2	2	[10]
		-	99.7	1000 cycles	1	1	1	
15	Au nanoparticle	106	-	2000 h	0.25	0.05	0.25	[11]
		-	97.1	60 cycles	0.03	0.5	0.5	
16	$AgZn_3$@Zn	43.1	-	1150 h	0.575	1	1	[12]
17	$Zn_{88}Al_{12}$	20		2000 h	0.5	0.5	0.5	[13]
18	Fe_2O_3	20	-	1000 h	0.05	0.05	0.1	[14]
19	In	54	-	1500 h	0.15	0.2	0.2	[15]
20	Cu/Zn	46	-	1500 h	0.75	0.5	1	[16]
		-	91.8	100 cycles	0.05	0.5	5	
21	COFs	36	-	420 h	0.21	1	1	[17]
		-	99.95	120 cycles	0.0684	0.57	1.13	
22	FCOF	60	-	1700 h	4.25	1	5	[18]
		-	97.2	320 cycles	0.32	1	80	
23	Sn	50	-	500 h	0.25	0.5	1	[19]
24	ZnSe	41	-	1530 h	0.765	1	1	[20]
		-	99.2	320 cycles	0.32	1	80	
25	$Zn_3(PO_4)_2{\cdot}4H_2O$	60	-	1200 h	0.6	1	1	[21]
		-	99.4	400 cycles	-	-	-	
26	EDTA anions	99	-	450 h	0.45	2	2	[22]
		-	99.5	700 cycles	0.7	1	2	
27	MoS_2	120	-	160 h	0.2	0.416	2.5	[23]
28	Ni_5Zn_{21}	47	-	2200 h	2.2	1	2	[24]
29	ZnP	25	-	3300 h	3.3	0.5	2	[25]
		-	99.5	200 cycles	0.1	0.5	2	
30	ZnO	22.2	-	1000 h	0.1	0.2	0.2	[26]
31	ZnF_2	71.5	-	800 h	0.4	1	1	[27]
		-	99.5	1000 cycles	1	1	5	
32	Kaolin	70	-	800 h	1.76	1.1	4.4	[28]
33	NTP	30	-	260 h	0.13	1	1	[29]

34	Barium titanate	36	-	840 h	0.21	0.5	0.5	[30]
35	PVDF-Sn@Zn	~30	-	200 h	1	10	10	[31]
		-	99	500 cycles	0.5	1	5	
36	ZF@F-TiO_2	~20	-	460 h	0.23	1	1	[32]
37	Sb@Cu	20	97.8	700 h	1.25	5	5	[33]
		-	98.0	550 h	5.5	10	20	
38	Ag@SS	29	99.8	640 h	3.2	1	10	[34]
39	Cu NBs@NCFs	63.2	98.8	400 h	1	1	5	[35]
40	CoCC	65	-	80 h	0.8	1	20	[36]
41	O, N-CC	16.7	98.7	320 h	0.16	1	1	[37]
42	Sn@NHCF	11.4	99.7	200 h	0.5	5	5	[38]
43	Zn@SCF	27	98.25	179 h	0.0895	1	1	[39]
44	Zn-Ti	27	-	1300 h	0.65	1	1	[40]
		-	99.60	3000 cycles	4	1	5	

*Surface engineering: 6-36; Current collectors engineering: 37-43; Structural engineering: 44.

Supplementary Table S2 ICP-OES/MS results under different conditions.

Sample	Conditions	Element (Bi)	
		C (mol/L)	ppm (mg/L)
1	Soaking in 2 M $ZnSO_4$ for 7 day	0.0000291894	0.0061
2	After plating under 5 mA cm^{-2} for 1h	0.0000293503	0.006134
3	After stripping under 5 mA cm^{-2} for 1h	0.000119629	0.025

References

1. J. Ding, Y. Liu, S. Huang, X. Wang, J. Yang, L. Wang, M. Xue, X. Zhang and J. Chen, ACS Appl. Mater. Interfaces, 2021, 13, 29746-29754.
2. X. Zhou, P. Cao, A. Wei, A. Zou, H. Ye, W. Liu, J. Tang and J. Yang, ACS Appl. Mater. Interfaces, 2021, 13, 8181-8190.
3. L. Dai, T. Wang, B. Jin, N. Liu, Y. Niu, W. Meng, Z. Gao, X. Wu, L. Wang and Z. He, Surf. Coat. Technol., 2021, 427, 127813.
4. Y. Yang, C. Liu, Z. Lv, H. Yang, X. Cheng, S. Zhang, M. Ye, Y. Zhang, L. Chen, J. Zhao and C. C. Li, Energy Stor. Mater., 2021, 41, 230-239.
5. L. Tan, C. Wei, Y. Zhang, Y. An, S. Xiong and J. Feng, Chem. Eng. J., 2022, 431, 134277.
6. L. T. Hieu, S. So, I. T. Kim and J. Hur, Chem. Eng. J., 2021, 411, 128584.
7. J. Hao, X. Li, S. Zhang, F. Yang, X. Zeng, S. Zhang, G. Bo, C. Wang and Z. Guo, Adv. Funct. Mater., 2020, 30, 2001263.
8. C. Ma, X. Wang, W. Lu, C. Wang, H. Yue, G. Sun, D. Zhang and F. Du, Chem. Eng. J., 2022, 429, 132576.
9. R. Zhao, Y. Yang, G. Liu, R. Zhu, J. Huang, Z. Chen, Z. Gao, X. Chen and L. Qie, Adv. Funct. Mater., 2021, 31, 2001867.
10. H. Du, R. Zhao, Y. Yang, Z. Liu, L. Qie and Y. Huang, Angewandte Chemie International Edition, 2022, 61, e202114789.
11. M. Cui, Y. Xiao, L. Kang, W. Du, Y. Gao, X. Sun, Y. Zhou, X. Li, H. Li, F. Jiang and C. Zhi, ACS Applied Energy Materials, 2019, 2, 6490-6496.
12. H. Lu, Q. Jin, X. Jiang, Z.-M. Dang, D. Zhang and Y. Jin, Small, 2022, 18, 2200131.
13. S.-B. Wang, Q. Ran, R.-Q. Yao, H. Shi, Z. Wen, M. Zhao, X.-Y. Lang and Q. Jiang, Nat. Commun., 2020, 11, 1634.
14. Z. Zeng, Y. Zeng, L. Sun, H. Mi, L. Deng, P. Zhang, X. Ren and Y. Li, Nanoscale, 2021, 13, 12223-12232.
15. D. Han, S. Wu, S. Zhang, Y. Deng, C. Cui, L. Zhang, Y. Long, H. Li, Y. Tao, Z. Weng, Q.-H. Yang and F. Kang, Small, 2020, 16, 2001736.
16. Z. Cai, Y. Ou, J. Wang, R. Xiao, L. Fu, Z. Yuan, R. Zhan and Y. Sun, Energy Stor. Mater., 2020, 27, 205-211.
17. J. H. Park, M.-J. Kwak, C. Hwang, K.-N. Kang, N. Liu, J.-H. Jang and B. A. Grzybowski, Adv. Mater., 2021, 33, 2101726.
18. Z. Zhao, R. Wang, C. Peng, W. Chen, T. Wu, B. Hu, W. Weng, Y. Yao, J. Zeng, Z. Chen, P. Liu, Y. Liu, G. Li, J. Guo, H. Lu and Z. Guo, Nat. Commun., 2021, 12, 6606.
19. W. Guo, Y. Zhang, X. Tong, X. Wang, L. Zhang, X. Xia and J. Tu, Mater. Today Energy, 2021, 20, 100675.
20. X. Yang, C. Li, Z. Sun, S. Yang, Z. Shi, R. Huang, B. Liu, S. Li, Y. Wu, M. Wang, Y. Su, S. Dou and J. Sun, Adv. Mater., 2021, 33, 2105951.
21. X. Zeng, J. Mao, J. Hao, J. Liu, S. Liu, Z. Wang, Y. Wang, S. Zhang, T. Zheng, J. Liu, P. Rao and Z. Guo, Adv. Mater., 2021, 33, 2007416.
22. S.-J. Zhang, J. Hao, D. Luo, P.-F. Zhang, B. Zhang, K. Davey, Z. Lin and S.-Z. Qiao, Adv. Energy Mater., 2021, 11, 2102010.
23. S. Bhoyate, S. Mhin, J.-e. Jeon, K. Park, J. Kim and W. Choi, ACS Appl. Mater. Interfaces, 2020, 12, 27249-27257.
24. P. Cao, J. Tang, A. Wei, Q. Bai, Q. Meng, S. Fan, H. Ye, Y. Zhou, X. Zhou and J. Yang, ACS Appl. Mater. Interfaces, 2021, 13, 48855-48864.
25. P. Cao, X. Zhou, A. Wei, Q. Meng, H. Ye, W. Liu, J. Tang and J. Yang, Adv. Funct. Mater., 2021, 31, 2100398.
26. J. Y. Kim, G. Liu, G. Y. Shim, H. Kim and J. K. Lee, Adv. Funct. Mater., 2020, 30, 2004210.
27. Y. Yang, C. Liu, Z. Lv, H. Yang, Y. Zhang, M. Ye, L. Chen, J. Zhao and C. C. Li, Adv. Mater., 2021, 33, 2007388.
28. C. Deng, X. Xie, J. Han, Y. Tang, J. Gao, C. Liu, X. Shi, J. Zhou and S. Liang, Adv. Funct. Mater., 2020, 30, 2000599.
29. M. Liu, J. Cai, H. Ao, Z. Hou, Y. Zhu and Y. Qian, Adv. Funct. Mater., 2020, 30, 2004885.

30. C. Xie, Q. Zhang, Z. Yang, H. Ji, Y. Li, H. Li, L. Fu, D. Huang, Y. Tang and H. Wang, Chin. Chem. Lett., 2022, 33, 2653-2657.
31. Q. Cao, Y. Gao, J. Pu, X. Zhao, Y. Wang, J. Chen and C. Guan, Nat. Commun., 2023, 14, 641.
32. Q. Zhang, J. Luan, X. Huang, Q. Wang, D. Sun, Y. Tang, X. Ji and H. Wang, Nat. Commun., 2020, 11, 3961.
33. X. Zheng, Z. Liu, J. Sun, R. Luo, K. Xu, M. Si, J. Kang, Y. Yuan, S. Liu, T. Ahmad, T. Jiang, N. Chen, M. Wang, Y. Xu, M. Chuai, Z. Zhu, Q. Peng, Y. Meng, K. Zhang, W. Wang and W. Chen, Nat. Commun., 2023, 14, 76.
34. Y. Zhang, G. Wang, F. Yu, G. Xu, Z. Li, M. Zhu, Z. Yue, M. Wu, H.-K. Liu, S.-X. Dou and C. Wu, Chem. Eng. J., 2021, 416, 128062.
35. Y. Zeng, P. X. Sun, Z. Pei, Q. Jin, X. Zhang, L. Yu and X. W. Lou, Adv. Mater., 2022, 34, 2200342.
36. H. Li, C. Guo, T. Zhang, P. Xue, R. Zhao, W. Zhou, W. Li, A. Elzatahry, D. Zhao and D. Chao, Nano Lett., 2022, 22, 4223-4231.
37. M. Zhou, G. Sun and S.-Q. Zang, J. Energy Chem., 2022, 69, 76-83.
38. H. Yu, Y. Zeng, N. W. Li, D. Luan, L. Yu and X. W. Lou, Sci. Adv., 8, eabm5766.
39. B. Cui, Y. Gao, X. Han and W. Hu, J. Mater. Sci. Technol., 2022, 117, 72-78.
40. Y. Zhao, S. Guo, M. Chen, B. Lu, X. Zhang, S. Liang and J. Zhou, Nat. Commun., 2023, 14, 7080.